Steel and Composite Structures, *Vol. 18, No. 4 (2015) 1023-1044*
DOI: http://dx.doi.org/10.12989/scs.2015.18.4.1023

Efficiency of stiffening plates in fabricated concrete-filled tubes under monotonic compression

Albert Albareda-Valls * and Jordi Maristany Carreras [a]

Technical University of Catalonia, Structures in Architecture, Av. Diagonal 649 Barcelona 08028, Spain

(*Received July 17, 2014, Revised October 01, 2014, Accepted October 23, 2014*)

Abstract. Concrete-filled tubes (CFT), formed by an outer steel tube filled with plain or reinforced concrete inside, have been increasingly used these recent decades as columns or beam-columns, especially for tall buildings in seismic areas due to their excellent structural response. This improved behavior is derived from the effect of confinement provided by the tube, since the compressive strength of concrete increases when being subjected to hydrostatic pressure. In circular CFTs under compression, the whole tube is uniformly tensioned due to the radial expansion of concrete. Contrarily, in rectangular and square-shaped CFTs, the lateral flanges become subjected to in-plane bending derived from this volumetric expansion, and this fact implies a reduction of the confinement effect of the core. This study presents a numerical analysis of different configurations of CFT stub columns with inner stiffening plates, limited to the study of the influence of these plates on the compressive behavior without eccentricity. The final purpose is to evaluate the efficiency in terms of strength and ductility of introducing stiffeners into circular and square CFT sections under large deformation axial loading.

Keywords: axial compression; concrete-filled steel tubes; numerical analysis; design codes; composite structures

1. Introduction

Concrete-Filled Tube sections (CFT) have been increasingly used in recent years as columns or beam-columns, especially in tall buildings, due to their improved ductility and strength. These mechanical properties come from the combination of steel and concrete. CFT sections constitute one curious case of "symbiosis" between two materials, similar to those associations of organisms in nature: concrete strength is enhanced by the tube, while steel is partially restricted against local buckling (Chacón *et al*. 2012). The result is a very versatile sectional typology, with high mechanical strengths and *ease* of construction. CFT sections have been studied from several points of view by renowned experts, especially under compressive loading (as it is the most beneficial way of loading). Schneider (1998) carried out a collection of experimental tests on CFT sections and other researchers did the same for bending (Elchalakani *et al*. 2001) and shear. The most important issue dealing with compression has been the confinement effect of concrete provided by

∗Corresponding author, Ph.D., E-mail: albert.albareda@upc.edu
[a] Ph.D., E-mail: Jordi.maristany@upc.edu

http://www.techno-press.org/?journal=scs&subpage=8 ISSN: 1229-9367 (Print), 1598-6233 (Online)

the tube, so that the behavior of concrete under high hydrostatic pressures plays a significant role.

The case of circular CFT sections is really different from square or rectangular-shaped ones, since this confinement is significantly higher in the first group due to the uniform distribution of pressure. This is the reason why several researchers have been focused on exploring different alternatives to stiffen the flanges of square sections in order to preserve the confinement effect. One of the alternatives consists in introducing welded bars inside the tube, so that they play the role of stiffeners. Hu *et al*. (2003) have been carrying out research and tests about the efficiency of stiffening bars, and also others worked in the same direction: Huang *et al*. (2002), Liu *et al*. (2002), Nassem Baig *et al*. (2006) and Cai and Long (2009). Tao *et al*. (2005) have been working these last years with some experts as B. Uy and L.H. Han regarding to the influence of these bars inside CFT square and rectangular sections (Tao *et al*. 2007) and (Tao *et al*. 2009). From all these experiments, it is derived that square-shaped CFT sections stiffened with bars tend to behave similar to circular sections under compression.

A similar alternative to these stiffening bars has emerged these last recent years, consisting in replacing the bars by entire inner stiffening plates (Fig. 1); this solution comes from Japan, proposed by Yamao *et al*. (2002) and Zhanfei and Yamao (2011) for hollow steel tubes, and it has been already used in some real bridges. No studies exist yet about which influence could these plates have in case of composite sections. Besides no specific experiments have been carried out, especially due to the fact that this is a solution thought for columns with significant diameters for bridge piers or tall buildings (starting from 400 mm). Zhanfei and Yamao (2011) analyzed the behavior of partially stiffened sections under cyclic loading, but he did not compare the efficiency of this proposal versus the alternative of proposing a thicker tube. The paper which is proposed here aims to describe the advantages and the efficiency of introducing stiffening plates in circular and square-shaped CFT sections under large deformation axial loading (up to the collapse of the section).

Derived from the need of new geometries, Ren *et al*. (2014) tested a set of 44 CFT specimens with unusual shapes under compression. Some of the tested sections come from circular sections (1/4 and 1/2 tube, for example), in order to know how lateral pressure is distributed in smaller alveoli and combining circular and square shapes.

It is clear that the introduction of internal plates in tubular sections is not especially trouble-free from a strictly practical point of view. The prescription of these plates should obey a clear concept of structural efficiency in terms of strength and ductility, which could compensate the significant

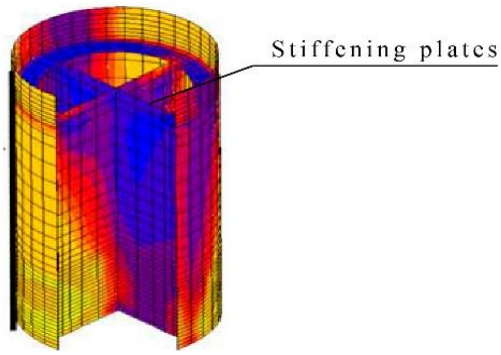

Fig. 1 FE model of stiffened specimen CR8330 analysed by Zhanfei and Yamao (2011)

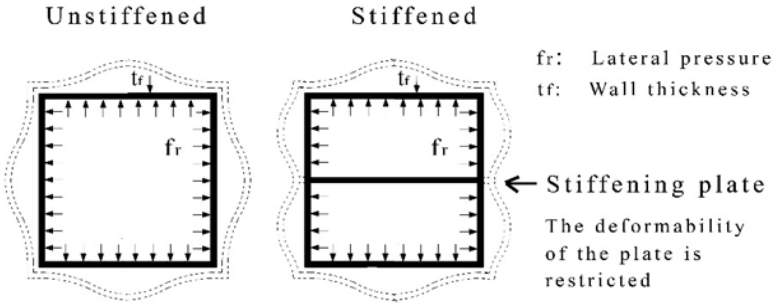

Fig. 2 Stiffening plates in square-shaped tubes limit the deformability of the flanges, while in circular tubes it seems to not be significant

effort of welding or fixing the plates to the tube. This research aims to propose this particular solution for engineers and architects, especially for heavily loaded columns located in seismic areas.

2. The hypothesis

Concrete in circular CFT sections becomes usually confined by the steel tube, and this is a phenomenon due to the circular geometry of the tube, which allows a uniform distribution of pressure over the core. When concrete is subjected to relatively advanced stages of loading, the material starts to expand laterally much more than the expansion which is established by the elastic Poisson's ratio. This volumetric expansion during the plastic range is converted into a tensile hoop stress in the tube, thanks to this lateral pressure. However, this phenomenon mostly occurs in circular sections, thanks to the efficiency of the annular shape.

The confinement effect is less significant in square and rectangular-shaped sections, due to the deformability of the flanges of the tube (see Fig. 2). The lack of rigidity of the flanges in this case not only has a decisive influence on the confinement effect, but also on ductility: the introduction of embedded plates inside these tubes may improve both mechanical properties of the composite section. This study presents a numerical analysis of circular and square-shaped CFT sections, with and without stiffening plates, subjected to monotonic compression. The study shows a comparison between the results coming from stiffened and unstiffened sections (but always equivalent in terms of material).

3. Material properties and constitutive models

The paper presents a parametric study of 10 different cases based on a numerical analysis; for that purpose, S355 steel and C40 concrete have been assumed in order to reduce complexity. Since the specimens have been subjected to large deformation axial loading (up to the collapse of the sections), inelastic period has been obviously considered in both materials up to the failure. For that purpose, continuum models in ABAQUS software (version 6.10) have been used, with a multilinear elastic-plastic model with isotropic hardening for steel and a damaged plasticity model for concrete (DPC). Both constitutive models have been previously validated with real tests.

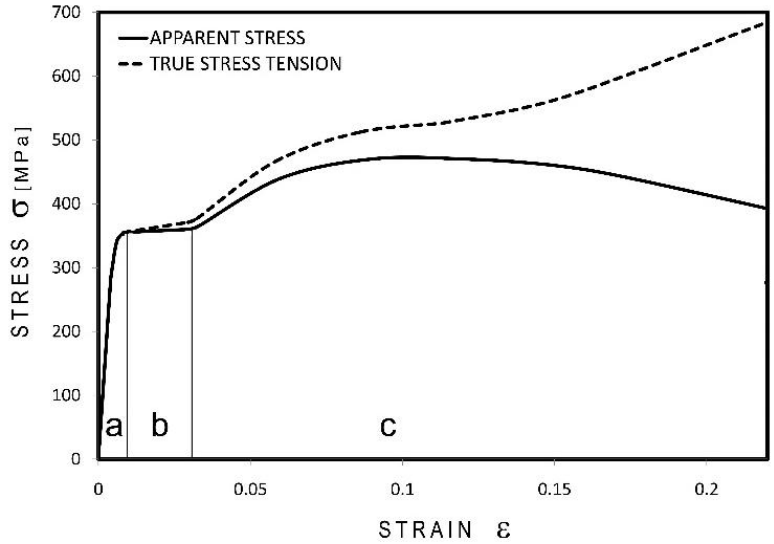

Fig. 3 Uniaxial true and engineering stress-strain curves for steel. Original engineering curve from Brockenbrough (1999), Section 1.1

3.1 Steel

A multilinear elastic-plastic model has been used for steel, by following the von Mises yield criterion with isotropic hardening. A monotonic uniaxial stress-strain curve has been introduced, with three different separated areas, according to the structural response of the material: (a) the elastic zone; (b) the yield plateau; and (c) the strain hardening zone up to the fracture (see Fig. 3). The true stress-strain curve has been assumed instead of the engineering one; this option has been determinant in order to reproduce the influence of the hardening period of steel on the load-strain curve of the section. The initial Young modulus for steel has been assumed as 210.000 MPa, and the elastic Poisson's ratio, 0,29.

3.2 Concrete

Damage plasticity model for concrete (DPC) has been used to simulate the concrete behaviour. This is a three-dimensional continuum plasticity-based damage model that is capable of simulating both tensile and compressive concrete responses, including for the case of high confining pressures.

Two hardening laws (depending on the plastic strain rates) can be defined separately for tension and compression. Concrete in the inelastic range behaves different under tension than under compression, as it is shown in Fig. 4 shown below. In the plastic range, a damage process starts to degrade the stiffness matrix of the material, and it is expressed by a scalar coefficient d_c which represents the percentage of cracked or crushed concrete, (Lubliner and Oller 1985). In CFT sections, this process depends not only on the hydrostatic pressure, but also on the geometry of the filling tube. This is the reason why the most difficult point when simulating the behaviour of concrete embedded in tubes is to predict the slope of the softening loading curve, as well as the residual stress.

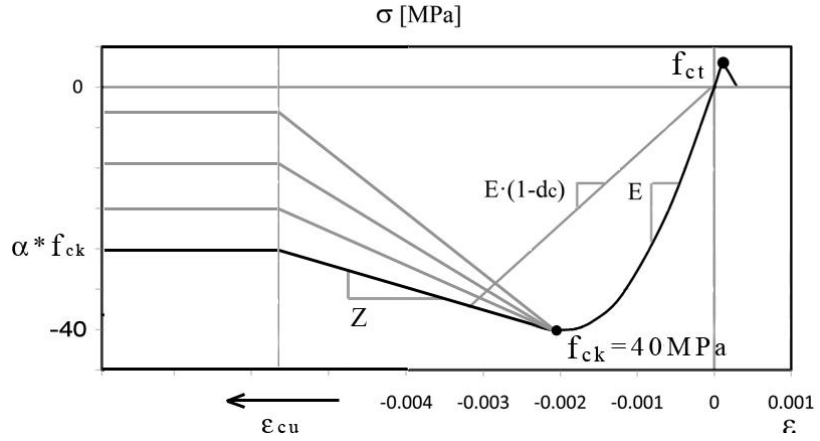

Fig. 4 Uniaxial stress-strain curve used for concrete. The post-peak behaviour has been determined according to Susantha *et al*. (2000)

The expressions given by Susantha *et al*. (2000) were used in this study to modify the post-peak period of the stress-strain curves, depending on the shape and the thickness of the tubes. Susantha *et al*. (2000) proposed some simplified expressions to describe the softening curve after the peak, using the results from more than 40 experiments with different shapes.

In this study, the first period of the compressive stress-strain curve has been always fixed up to the maximum strength of concrete (f_{ck} = 40 MPa) for all specimens, while the softening period has been defined according to Susantha's model. These expressions provide a value for the softening slope (Z) and the residual stress strain (ε_{cu}) (see Fig. 4) depending on the geometry of the tube and the material properties of each section.

The expressions given by Susantha *et al*. (2000) which have been used are shown below Eqs. (1)-(4), depending on the radius-to-thickness parameter

$$R_t = \sqrt{3(1-\nu^2)}\,\frac{f_y}{E_s}\,\frac{D}{2t} \tag{1}$$

The following criteria for circular CFT sections have been used to compute parameters Z and ε_{cu}

$$Z = \begin{cases} 0 & \text{if} \quad R_t(f_c'/f_y) \le 0.006 \\ 1.0\times10^6 R_t(f_c'/f_y) - 6000 & \text{if} \quad R_t(f_c'/f_y) \ge 0.006 \end{cases} \tag{2}$$

$$\varepsilon_{cu} = 0.025 \tag{3}$$

Similar expressions for square-shaped sections have been also implemented

$$Z = \begin{cases} 0 & \text{if} \quad R_t(f_c/f_y) \le 0.0039 \\ 23.,400\times R_t(f_c/f_y) - 91.26 & \text{if} \quad R_t(f_c/f_y) > 0.0039 \end{cases} \tag{4}$$

$$\varepsilon_{cu} = \begin{Bmatrix} 0.04 & \text{if} \quad R_t(f_c/f_y) \le 0.042 \\ 14.50*\left[R_t(f_c/f_y)\right]^2 - 2.4*R_t(f_c/f_y) + 0.116 & \text{if} \quad 0.042 < R_t(f_c/f_y) < 0.073 \\ 0.018 & \text{if} \quad R_t(f_c/f_y) \ge 0.073 \end{Bmatrix} \tag{5}$$

To compute these values for stiffened specimens, the parameter D of the radius-to-thickness ratio has been assumed as the smaller dimension of the resulting cell in square sections, while in case of circular sections, as the outer section diameter. These assumptions have been done in order to obtain the accurate results as possible.

On the other hand, the maximum tensile yield stress for concrete f_{ct} has been considered as 9% of the maximum characteristic compressive stress, and the elastic Poisson's ratio has been assumed as an initial value of 0.20. The initial modulus of elasticity of concrete derives from the following experimental expression in literature

$$E = 4700 \times \sqrt{f_{ck}} \tag{6}$$

As it is known, the DPC model allows defining the yield surface by means of the two parameters K_c and σ_{b0}/σ_{c0}: the first one describes the shape of the deviatoric plane, while the latter describes the ratio between the initial equibiaxial to the uniaxial compressive yield stress. A non-associated flow rule is used and the flow potential follows the Drucker-Praguer hyperbolic function. The dilation angle proposed is in this case 31º and the viscosity parameter is defined clearly small (close to zero) in order to allow stresses outside the yield surface and to avoid this way convergence difficulties.

In this case, the dilation angle is a decisive parameter to reproduce the effect of confinement over concrete, since it determines the volumetric expansion in the inelastic period. With a wrong value of this parameter, concrete in the model would not achieve the peak of load as steel expands more than concrete in the elastic range. This parameter has been determined by using the existing literature such as Jankowiak and Lodygowsky (2005), and Susantha *et al*. (2000). The last one proposes a formula to determine the *apparent* Poisson's ratio of a CFT, ν_e

$$\nu_e = 0.2312 + 0.3582 \times \nu_e' - 0.1524*\left(f_c/f_y\right) + 4.843 \times \nu_e' \times \left(f_c/f_y\right) - 9.169 \times \left(f_c/f_y\right)^2 \tag{7}$$

$$\nu_e' = 0.881*10^{-6} \times (D/t)^3 - 2.58 \times 10^{-4} * (D/t)^2 + 1.953 \times 10^{-2} \times (D/t) + 0.4011 \tag{8}$$

Considering that the values coming from expression (2) range between 0.72 to 0.85 for D/t ratios between 20 and 60 in case of C40 concrete and S355 steel, a value of 31° was finally adopted according to a preliminary analysis by using a cylindrical specimen of 150 × 300 mm (D × H) with an equivalent lateral pressure f_{rp} = 6 MPa (from Eq. (9)), simulating an outer tube with D/t = 30. The lateral expansion varied depending on this parameter (see Fig. 5).

$$f_{rp} = (\nu_e - \nu_s) \times (2t \times f_y) / (D - 2t) \tag{9}$$

4. Features of the model

4.1 Element type

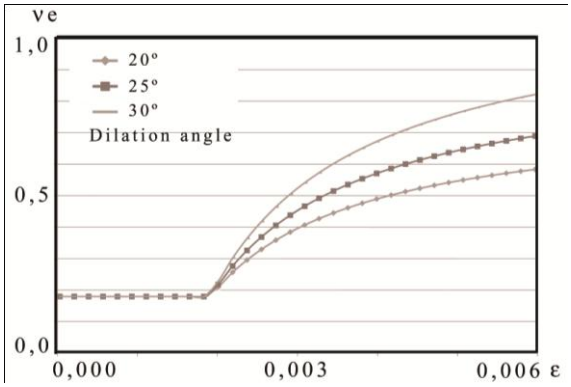

Fig. 5 Variation of the *apparent* Poisson's ratio depending on the dilation angle. The analysis has been done assuming a lateral pressure of 6 MPa in a cylindrical specimen

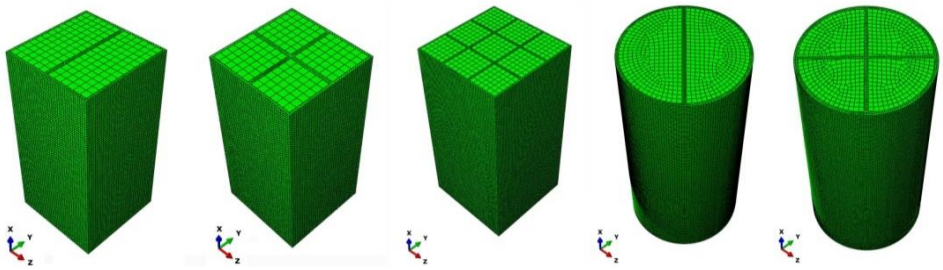

Fig. 6 Different analysed typologies, with their respective meshes

The three-dimensional brick element, C3D8, available also in ABAQUS, has been used for all the models. A fine hex mesh has been chosen for the analysis in order to use solid elements to model both concrete core and steel plates. The final element proportions have been determined by evaluating results from different finite element models. In the meshes chosen in this study, three or more elements have been used through the wall-thickness of all steel components in order to consider possible stress variations, and being the steel elements approximately 3 to 4 times smaller than the specimen's width (see Fig. 6).

4.2 Size and boundary conditions

The size and boundary conditions of the tested specimens are also important factors in this analysis. Similar conditions shown by real experiments have been used in the numerical models, in order to be capable of comparing and validating the results. With this objective, specimens used for validation and those for the parametric study have a height to width ratio about 2, being all restricted against rotation at the upper face and also against vertical displacement at the base. These conditions reproduce those of experiments in laboratory to reproduce the same behaviour and failure mode.

4.3 Interaction properties

The interaction properties have been assumed by enabling surface-to-surface contact between

the steel and concrete instances. The model which has been used is capable of transferring both normal and shear stresses.

For normal stresses, the "hard contact" option has been chosen to determine whether contact takes place between steel and concrete or not; for tangential stresses, a constant friction coefficient has been established with an initial allowable elastic slip (Hajjar *et al.* 1998). The friction coefficient has been assumed with a value of 0.20, with a critical maximum value of transferred shear stresses depending on the shape and according to (Eurocode 4 2004), which is 0.40 MPa for filled tubes.

5. Validation of the model

The model has been validated by using real experimental tests of CFT sections under compression published by other researchers, and classified later by Susantha *et al.* (2000). To validate the finite element model is especially imperative at three different points along the load-strain diagram: the peak of load, the subsequent softening of concrete, and the hardening period of steel.

The achievement of the peak of load by using the numerical model is especially important in order to confirm that concrete is expanding properly, so that interaction between both materials is correct. Besides, during the post-peak period, it is also necessary to verify whether the confinement pressure keeps constant or not. As confinement effect depends not only on the loading stage, but also on the shape of the tube, the simplified formulation proposed by Susantha *et al.* (2000) to describe the post-peak behaviour in CFT sections has been implemented in the uniaxial stress-strain curves which have been used in this study, depending on the geometry of the section. Diagrams in Figs. 7-10 compare the experimental versus the numerical curves obtained in this analysis for a set of different circular and square-shaped sections. Eight different sections with different diameters and thicknesses have been used for validating the model, and a good agreement with experimental tests can be globally observed (Tables 1-2).

While N_{EXP} is the maximum compressive load coming from the experimental test, N_{FEM} corresponds to the maximum load derived from the numerical model which is used in this study. The same agreement of results is shown in the diagrams of Figs. 7 to 10, where two load-strain curves are superimposed: one coming from the numerical model (continuous line) and the other one from experimental test (dashed line). A very good accuracy is obtained from the numerical results, since these sections are circular and square-shaped and the post-peak behavior has been defined according to Susantha expressions. The only specimen which shows a significant difference (15%) between numerical and experimental results is 4 MN (see fig. 10), since

Table 1 Circular CFT sections used for verification Susantha *et al.* (2000)

Section	D* (mm)	t* (mm)	D/t	fy* (MPa)	fc* (MPa)	N_{exp*} (kN)	N_{FEM}* (kN)	N_{FEM}/N_{exp}	Mean	COV
3 MN	150.00	3.20	46.87	287.7	22.0	937.1	883.4	0.942	1.003	0.059
4 HN	150.00	4.00	37.50	279.9	28.7	1205.4	1229.4	1.019		
CC4-C-4	300.20	2.96	101.42	283.0	40.5	3394.3	3564.1	1.050		
CF4-CC40	318.50	7.90	40.32	358.1	47.5	6524.7	6544.0	1.002		

Table 2 Square-shaped CFT sections used for verification (Susantha *et al*. 2000)

Section	B (mm)	t (mm)	B/t	fy (MPa)	fc (MPa)	N_{exp} (kN)	N_{FEM} (MPa)	N_{FEM} / N_{exp}	Mean	COV
S5	126.80	7.47	16.97	347.0	23.8	1550.5	1635.4	1.054	1.043	0.076
S3	126.90	4.55	27.89	322.0	23.8	1074.7	1078.2	1.003		
CR4-A-4	148.20	4.38	33.83	261.2	40.5	1484.4	1432.8	0.965		
4 MN	150.00	4.30	34.90	279.9	18.1	1114.2	1281.5	1.150		

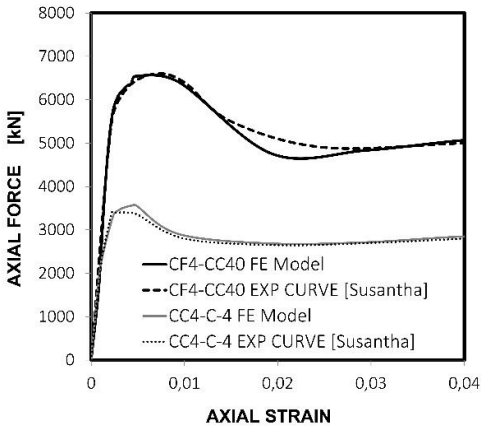

Fig. 7 Validation with specimens CF4-CC40, CC4-C-4

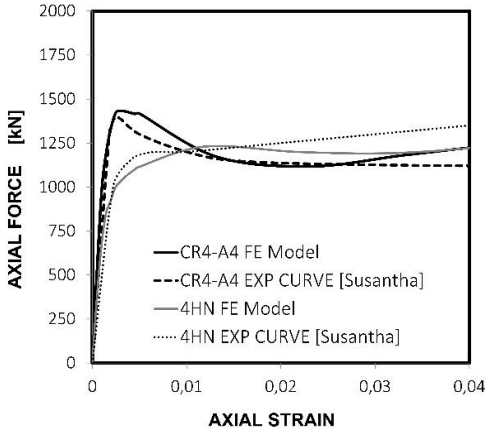

Fig. 8 Validation with specimens CR4-A4, 4HN

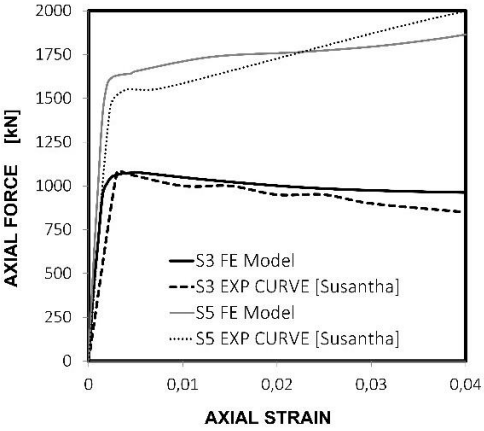

Fig. 9 Validation with specimens S3, S5

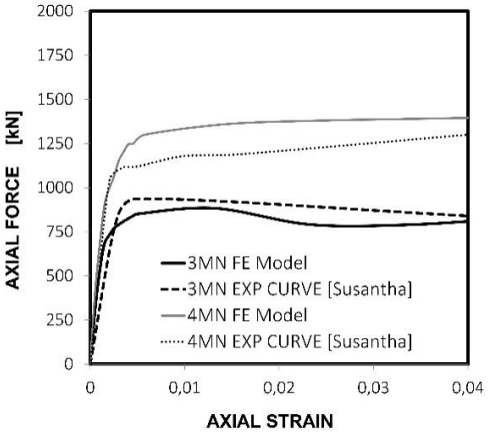

Fig. 10 Validation with specimens 3 MN, 4 LN

contrarily to others it is composed by low-strength concrete. The maximum confined compressive strength f_{cc} which is achieved by concrete in each case is very sensitive to the parameters used in the constitutive model, and a validated dilation angle of 25 MPa concrete was used also in this case. This is the reason of the difference in the results shown below.

Table 3 1/4 of circular sections used for verification (Ren *et al*. 2014)

Section	D^* (mm)	t^* (mm)	D/t	fy^* (MPa)	fc^* (MPa)	N_{exp^*} (kN)	$N_{FEM}{}^*$ (kN)	N_{FEM} / N_{exp}	Mean	COV
1/4c1-1	145.09	2.92	49.68	389.3	61.4	1634.0	1491.0	0.912	0.914	0.003
1/4c2-1	145.09	3.71	39.10	389.3	61.4	2060.0	1890.0	0.917		

As it is derived from the diagrams shown before, the use of the formulation proposed b Susantha *et al*. (2000) in the stress-strain curve for concrete of the numerical model is especially useful in order to reproduce the softening of CFT sections. The decrement of stress beyond the peak of load of these sections is very sensitive to the confinement effect and also to the geometry of the tube, as Susantha and others observed. A good simulation of the post-peak period is important to describe the ductility and the collapse of a CFT specimen. Ductility is here referred to the capacity of the section to deform under a compressive load before the ultimate load (where the collapse takes place).

In order to check the validity of the model also for the case of stiffened CFT sections, where there is no perfect lateral pressure distribution, some experiments carried out by Ren *et al*. (2014) have been also used. These authors tested more than 40 specimens with special shapes to know about the behaviour of concrete inside different tube geometries. However, it is obvious that the expressions proposed by Susantha were valid only for circular and square-shaped tubes, so that other shapes tend to behave slightly different. Table 3 shows the properties of two specimens used for validation, with a cross-sectional shape of 1/4 of a circular tube and Fig. 11 compares the obtained curves with the experimental ones.

There is a slight difference between numerical and experimental results in case of Ren *et al*. (2014) specimens, contrarily to others used for validation before (Figs. 7-10). This difference is due in part to the specific geometry of these sections (1/4 circular instead of pure circular), but especially due to the use of 60 MPa concrete instead of 40 MPa. To get a fine agreement at the peak of load, it is important to validate certain parameters such as the dilation angle, for each strength of concrete.

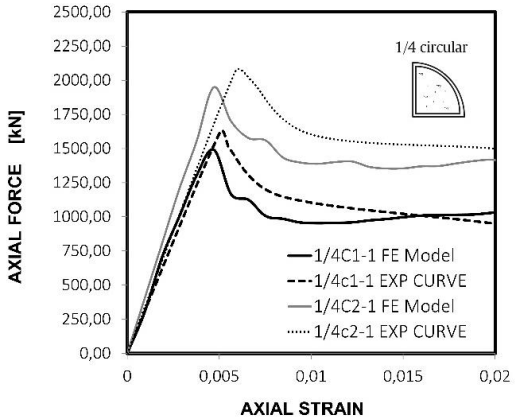

Fig. 11 Validation with specimens 1/4c1-1 and 1/4c2-1 carried out by Ren *et al*. (2014)

6. Numerical analysis

To describe the influence of stiffening plates in CFT tubes, five different configurations have been analysed depending on the number of internal stiffeners. This way, one and two plates have been considered in this analysis for circular sections, and also four plates in case of square CFT's (Fig. 12). Depending on the geometry and boundary conditions, 7 different cells have been detected in these configurations, which in practice correspond to 7 different patterns of confinement (named with letters from A to G). For example, while cell A is restricted only by one internal face, cells B and C are restricted by two internal faces; cell D is surrounded by three internal faces, and cell E becomes completely surrounded by internal stiffeners.

On the other hand, the proposed specimens have been named by using the code C or S for circular or square shapes, followed by the number of alveoli (2, 4 or 9). The first four resulting typologies C2, C4, S2 and S4 correspond to one or two-plate configurations, while the latter (S9) is only appropriate for heavily loaded columns. Since the introduction of these plates plays a decisive role on the deformability of the flanges of the tube, two different thicknesses have been also considered in the analysis (6 and 12 mm) to describe the influence of stiffeners depending on the B/t ratio. Contrarily, the outer size of the cells have been kept constant with a width of 200 mm, which is considered a reasonable reduced size to guarantee the confinement effect in square sections. Internal plates have been considered 1.2 times thicker than the outer ones, to improve the effect of stiffening on the flanges. All the analyzed specimens and their mechanical properties are shown below (Table 4).

Fig. 12 Different cells and typologies corresponding to different configurations of stiffening plates

Table 4 Stiffened CFT Sections

Specimen	*D* or *B* (mm)	t_{out} (mm)	t_{inn} (mm)	*D*/*t* or *B*/*t*
C2a	400.00	10.0	12.0	40.00
C2b	400.00	5.0	6.0	80.00
C4a	400.00	10.0	12.0	40.00
C4b	400.00	5.0	6.0	80.00
S2a	400.00	10.0	12.0	40.00
S2b	400.00	5.0	6.0	80.00
S4a	400.00	10.0	12.0	40.00
S4b	400.00	5.0	6.0	80.00
S9a	600.00	10.0	12.0	60.00
S9b	600.00	5.0	6.0	120.00

* *D* and B are the outer diameter or dimension

All sections are 400 mm width, except for the case of S9, which is 600 mm width in order to keep the same *B*/*t* ratio for internal cells (the cells are kept 200 mm width). A medium-strength concrete (40 MPa) and a regular-strength steel (355 MPa) have been used for all specimens only, since the hypothesis of this study is basically focussed on a geometrical issue. The influence of the material strengths and properties is not the scope of this investigation.

By combining the different obtained cells, lots of new geometrical configurations could be desi-gned, assuming also different percentages of confinement for each alveoli. The confinement pressu-re would depend on the thickness of the flanges, on the *B*/*t* ratio of the cell and on the position of this cell inside the cross-section area (boundary conditions).

7. Evaluation of efficiency

To evaluate the efficiency of the proposed stiffening plates in CFT sections subjected to monotonic compression, a parametric analysis has been done by comparing stiffened sections with other unstiffened ones, but equivalent in terms of area (with the same outer diameter or width, and the same amount of steel and concrete). This equivalence is obtained through an equivalent thickness, t_{eq}, which is implemented into a fixed-diameter circular (or square-shaped) section (see Fig. 13); in this way, the sections are fully equivalent in terms of material and cost. The purpose of this comparison is to determine the influence and the benefits of introducing these mentioned plates inside tubular composite sections, being subjected to compressive loads.

The equivalent sections which have been considered in the analysis are the following (Table 5).

Fig. 13 Equivalent circular and square sections proposed in this study

Table 5 Proposed equivalent specimens

Specimen	*D*/*B*	t_{eq} (mm)	*D*/*t* or *B*/*t**
C2a.eq	400.00	13.9	28.77
C4a.eq	400.00	17.7	22.59
S2a.eq	400.00	13.0	30.76
S4a.eq	400.00	16.0	25.00
S9a.eq	600.00	22.0	27.27
C2b.eq	400.00	6.9	57.97
C4b.eq	400.00	8.8	45.45
S2b.eq	400.00	6.5	61.53
S4b.eq	400.00	8.0	50.06
S9b.eq	600.00	11.0	54.54

*Depending on the geometry (circular or square)

Regarding to the distribution of longitudinal stresses along the column, different patterns of confinement can be detected. It is curious to see that as more stiffened becomes the section, more similar is the distribution of confinement effect over concrete to the one shown by a circular tube. However, in case of section S2 (which is clearly different in both axes) the lack of rigidity of two lateral flanges leads to a one-way confinement effect.

7.1 Efficiency regarding to maximum compressive strength

By comparing the results coming from the numerical analysis for stiffened circular sections, with those from their equivalent unstiffened specimens, it can be seen how surprisingly, the unstiffened group behaves better than the stiffened one (see Figs. 14 and 15). The maximum compressive strength is always higher for unstiffened sections with a pure circular geometry (see how the dashed line in Figs. 14 and 15 corresponding to the unstiffened sections achieves higher values of load in both cases).This enhancement becomes even more evident for thick-walled sections, since internal plates also help to delay and soften local buckling effects during the plastic

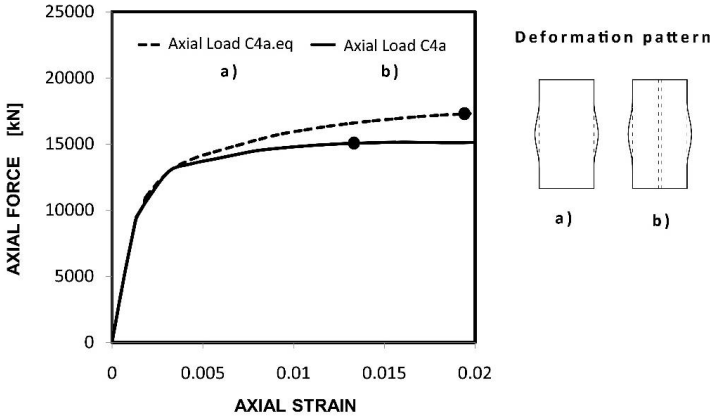

Fig. 14 Stiffened versus unstiffened section (C4a)

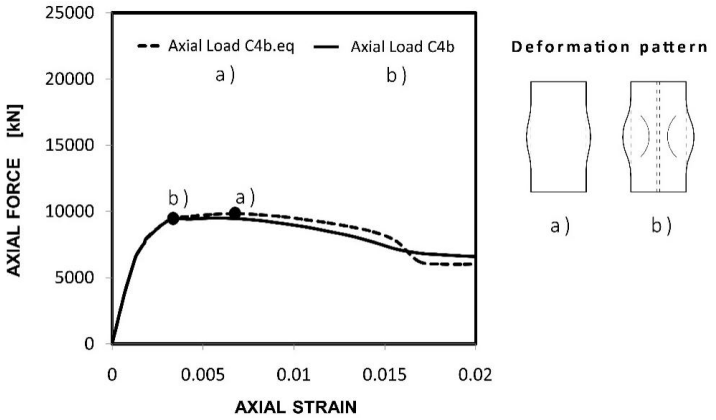

Fig. 15 Stiffened versus unstiffened section (C4b)

range. This phenomenon has a direct consequence on the application of these sections, since it becomes evident that stiffening plates are no especially convenient under pure compression.

This phenomenon can be explained by analyzing the geometry in the cross-sectional plane. By considering the deformed shape of stiffened sections C2 and C4 (see Fig. 16(b)), it is derived that internal plates generate slight parasite bending moments in the cross-sectional plane. The presence of specific points which are more rigid than the rest (those at the junction between the plate and the tube) leads to light negative and positive moments along the tube. The combination of stresses derived from bending moments and hoop tension in the wall-thickness implies that stresses in the tube are no longer uniformly distributed, and this is the reason why the section collapses earlier. If the stress is not uniform along the tube, the squash load of the section becomes also lower since the steel collapses locally before. Contrarily, in unstiffened circular sections (see Fig. 16(a)), the whole section becomes subjected to a tensile state as a result of the shape itself, and no bending moments occur in the cross-sectional plane. Thanks to this state, the efficiency of these tubes is higher, concerning to the effect of confinement over the core.

The case of square-shaped CFT sections is different, since the introduction of internal plates in this case becomes decisive in order to determinate the maximum compressive strength (see Figs. 17 and 18). Rectangular plates forming square tubes are quite deformable in its plane, derived

Fig. 16 Distribution of stresses in the wall-thickness of: (a) a circular tube; and (b) a stiffened circular tube

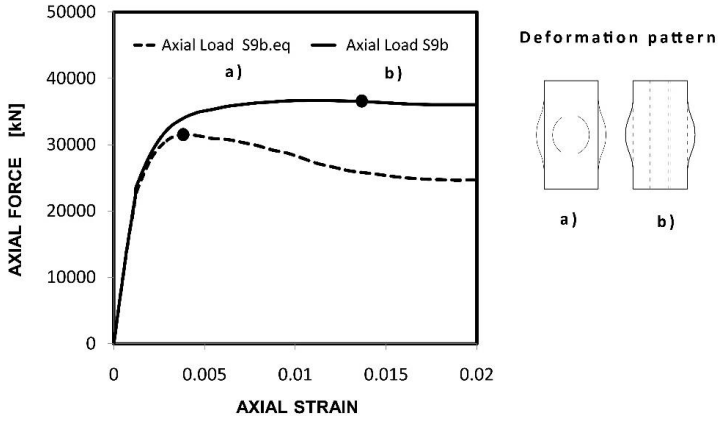

Fig. 17 Stiffened versus unstiffened section (S9a)

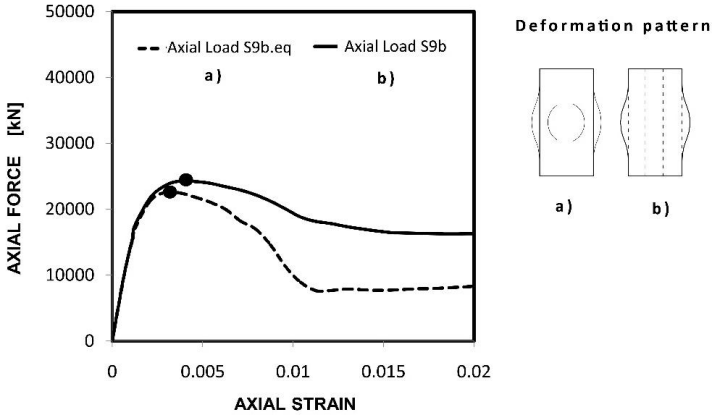

Fig. 18 Stiffened versus unstiffened section (S9b)

Table 6 Results of the FE model, corresponding to the analysis of efficiency

Unstiffened specimens	N_{peak} (kN)	f_{cc} (MPa)	ϕ	Stiffened specimens	N_{peak}' (kN)	f_{cc} (MPa)	ϕ'	ΔN (kN)
C2a.eq	14436.25	80.28	2.00	C2a	11715.32	55.27	1.38	-2720.94
C4a.eq	16771.96	88.71	2.21	C4a	15285.61	74.47	1.86	-1486.34
S2a.eq	13155.35	44.77	1.12	S2a	13373.50	46.33	1.16	**218.15**
S4a.eq	14554.99	45.05	1.12	S4a	17184.92	64.47	1.61	**2629.93**
S9a.eq	31250.10	43.83	1.09	S9a	37890.34	65.31	1.63	**6640.24**
C2b.eq	8424.06	48.25	1.20	C2b	8488.44	48.80	1.22	**64.38**
C4b.eq	9892.16	53.54	1.33	C4b	9703.96	51.90	1.29	-188.20
S2b.eq	9689.80	42.48	1.06	S2b	10345.75	46.86	1.17	**655.95**
S4b.eq	10423.47	41.68	1.04	S4b	11414.37	48.40	1.21	**990.90**
S9b.eq	22882.50	42.10	1.05	S9b	25470.95	49.84	1.24	**2588.44**

from their poor flexural stiffness. Due to lateral expansion of concrete, and as a consequence of their condition of flatness, they become subjected to important in-plane bending. This is the reason why stiffening plates in square CFT sections become seriously recommendable, as they restrict the deformability of the plates and may result in an enhancement of the compressive strength up to added percentages of 20% and more (see Table 6).

A list of numerical results is shown in Table 6. The influence of stiffening plates over CFT sections can be observed here, by comparing the grade of confinement over the core (ϕ, confinement in unstiffened sections and ϕ', confinement in stiffened sections, see Eq. 10). The value of f_{cc} (maximum confined compressive strength of concrete) is also reported here, and it is obtained as the average of vertical stresses in concrete from the FE model. Note that in case of circular sections, there is a decrement of strength (negative ΔN), while in case of square-shaped sections there is a clear increment.

$$\phi = \frac{f_{cc}}{f_c} \tag{10}$$

While the introduction of only 1 stiffening plate in square-shaped sections (Section S2) provides almost no extra confinement effect over the core, independently of the thickness, in cases of sections S4 and S9 with 2 and 4 embedded plates, this influence becomes much more evident (see Fig. 19). The shape of the resulting cell is very important to determine the enhancement of concrete strength; this is the reason why the increment of confinement effect in sections S4 and S9 is higher than in section S2. While cells in sections S4 and S9 are square-shaped, in section S2 the resulting cells are clearly rectangular: this is very important to guarantee this effect over the core, since two of the plates in section S2 are still clearly deformable despite the introduction of the stiffener. (a) In sections of group with thicker plates and tubes (t_{out} = 10 mm), (b) the effect of stiffening of the plates is clearly more significant than in those of group (t_{out} = 5 mm).

7.2 Efficiency regarding to ductility

Referring now to the influence of stiffening plates on the ductility of CFT sections, similar conclusions can be done from the FE results, being this influence more evident than in case of strength. For circular CFT sections, the presence of internal plates reduces the *energy of fracture* of the section, and consequently the ductility (see Table 7). The light bending moments which

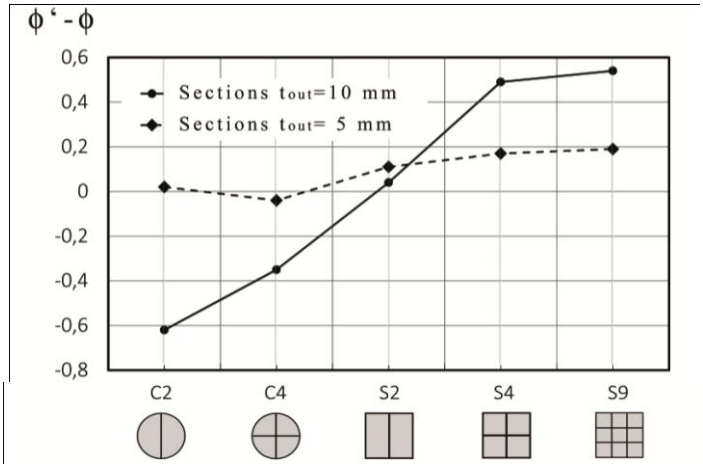

Fig. 19 Increment of confinement factor over concrete strength due to stiffening plates

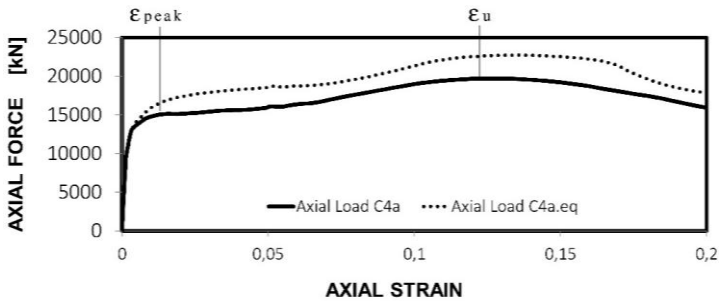

Fig. 20 Large deformation axial loading diagram for sections C4a and C4a.eq. (Thickness of the stiffened tube is 10 mm)

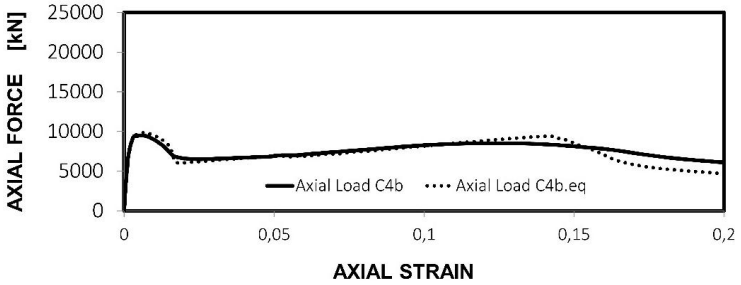

Fig. 21 Large deformation axial loading diagram for sections C4b and C4b.eq. (Thickness of the stiffened tube is 5 mm)

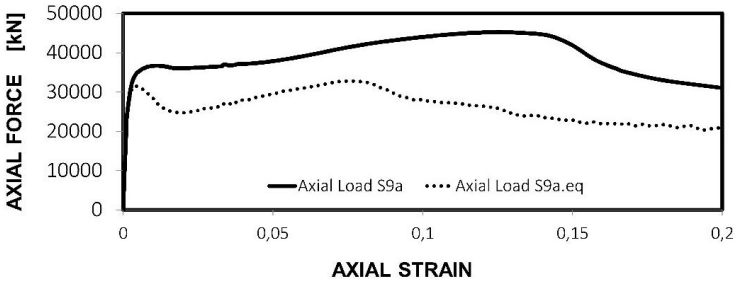

Fig. 22 Large deformation axial loading diagram for sections S9b and S9b.eq. (Thickness of the stiffened tube is 10 mm)

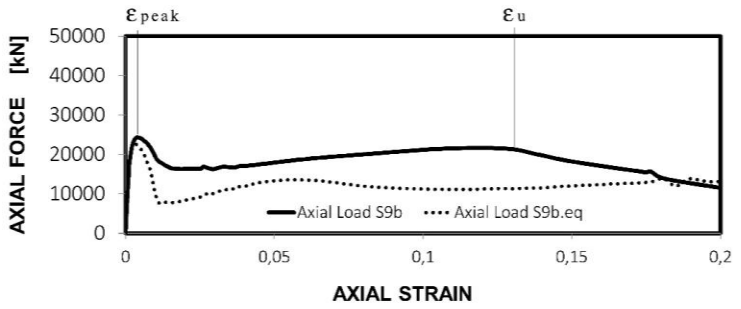

Fig. 23 Large deformation axial loading diagram for sections S9b and S9b.eq. (Thickness of the stiffened tube is 5 mm)

appear in the cross-section impedes the tube becoming uniformly tensioned, so that the maximum yield stress is only achieved in some specific points; thus, the failure of the specimen starts by these points, earlier than in unstiffened circular sections. Figs. 20 and 23 correspond to large deformation monotonic loading, up to the failure, for both stiffened and unstiffened sections with two different outer thicknesses.

As in terms of strength, the influence of stiffeners in square-shaped sections is more decisive. Note how section S9a notably improves its *energy of fracture* by eliminating the post-peak softening period, by introducing the embedded plates. After the peak of load, the stiffened section S9a keeps the load constant until the slope of the hardening period of steel arises. This effect takes also place in section S9b, although it is less significant.

Although stiffened square-shaped CFT sections fail later than the unstiffened ones, the failure occurs slightly sharper. The new configuration achieves that most part of the load can be retained until the ultimate strain, but at the same time the slope of the load-strain curve after the failure is also steeper. Values for the ultimate strain of stiffened and unstiffened sections are shown in Table 7 and are used to describe the concept of "ductility"; the parameter θ (Eq. 11) indicates the ratio between the ultimate and the peak strains (see Fig. 23) for unstiffened specimens. In the same way, parameter θ' indicates this ratio for stiffened specimens.

$$\theta = \frac{\varepsilon_u}{\varepsilon_{peak}} \tag{11}$$

By comparing the difference between parameters θ and θ' between different typologies, a significant decrement in circular sections is observed; on the contrary, a significant increment for square sections is also noted (curve of Fig. 24). The increment of ductility in stiffened square

Table 7 Peak and ultimate strains of analyzed specimens

Equivalent specimen	ε_{peak}	ε_u	θ	Stiffened specimen	ε'_{peak}	ε'_u	θ'
C2a.eq	0.004	**0.141**	35.0	C2a	0.009	**0.135**	15.0
C4a.eq	0.004	**0.136**	34.0	C4a	0.015	**0.127**	8.4
S2a.eq	0.004	**0.074**	18.5	S2a	0.004	**0.082**	20.5
S4a.eq	0.006	**0.095**	15.9	S4a	0.007	**0.135**	19.2
S9a.eq	0.009	**0.077**	8.5	S9a	0.018	**0.131**	7.2
C2b.eq	0.003	**0.152**	50.7	C2b	0.006	**0.145**	24.1
C4b.eq	0.003	**0.142**	47.3	C4b	0.009	**0.125**	13.8
S2b.eq	0.004	**0.079**	19.8	S2b	0.004	**0.112**	28.0
S4b.eq	0.005	**0.073**	14.6	S4b	0.005	**0.157**	31.4
S9b.eq	0.004	**0.056**	14.0	S9b	0.004	**0.129**	32.2

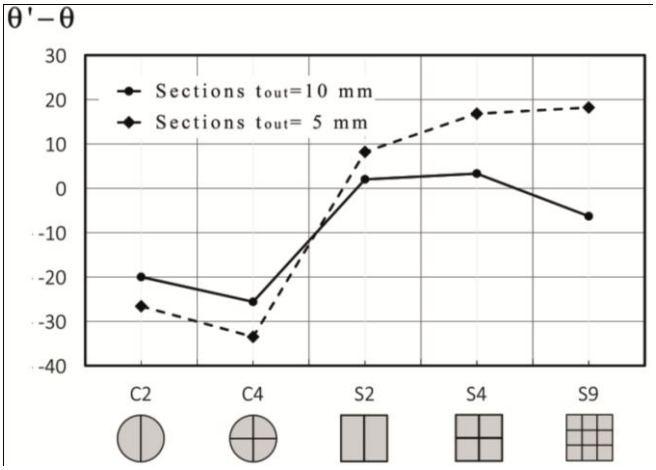

Fig. 24 Increment of confinement factor over concrete strength due to stiffening plates

(a) (b)

Fig. 25 (a) Deformation pattern of S9 before the collapse; (b) Lateral deformability of stiffening plates leads to an earlier collapse

sections can be explained by the deformation pattern of these sections (which is similar to circular ones); those strongly stiffened square sections (with one or more stiffening plates) tend to behave and collapse like circular concrete-filled tubes (see Fig. 25). Nevertheless, the descending slope in section S9 is significant: while the effect of confinement over concrete still grows from S4 to S9, the ductility of the latter becomes slightly reduced. This fact is mostly due to the eccentricity of the stiffeners respect to the centroid of the section; while in S2 and S4 the stiffening plates cross the centroid, in the geometry proposed by S9, the inner plates do not coincide with this point. In advanced stages of loading, the lateral expansion of concrete implies a lateral deformation of those plates which do not cross the centroid: in S9 all the plates accomplish this condition, so that the section collapses earlier than the rest by a geometric restriction itself (see Fig. 25(b)). We can say that section S9 allows more confinement over the core than sections S4 and S2, but at the same time it shows a sharper collapse.

This phenomena in those sections with an outer wall-thickness of 5 mm takes no place due to the global deformability of the flanges.

8. Evaluation of the results compared with EC-4

Eurocode 4 (2004) allows considering the confinement effect in circular CFT sections only. In these sections, the enhancement of the compressive strength of concrete depends on the slenderness ratio and the D/t and f_y/f_c ratios. By the contrary, this effect cannot be taken into account in square sections due to the lateral deformability of the plates. Nevertheless, this consideration is really conservative for low B/t ratios (Liu *et al*. 2003), where lateral plates are thick enough to provide also confinement to the core. In this way, the contribution of stiffeners is not considered in the EC-4 for any case. The following Table 8 shows a comparison between the obtained numerical values and those predicted by the Eurocode; it is important to highlight that to compute the EC-4 values no extra confinement coming from stiffeners has been taken into account, so that this effect has been only considered in circular sections directly derived from the circular shape.

Table 8 Results from the FE model compared with the EC-4

Stiffened specimens	N_{peak} (kN)	$N_{Eurocode}$ (kN)	$N_{peak} / N_{Eurocode}$	Mean	COV
C2a	11715.32	13684.30	0.856	0.940	0.126
C4a	15285.61	14918.69	1.024		
S2a	13373.50	10324.90	1.295	1.391	0.062
S4a	17184.92	11715.94	1.466		
S9a	37890.34	26782.02	1.414		
C2b	8488.44	9570.39	0.886	0.916	0.046
C4b	9703.96	10253.75	0.946		
S2b	10345.75	8389.22	1.233	1.238	0.009
S4b	11414.37	9114.98	1.252		
S9b	25470.95	20708.50	1.229		

This results show how conservative is the EC-4 to predict the compressive behavior of stiffened square CFT sections. The confinement effect provided by inner plates is not considered by the Eurocodes, although stiffened square-shaped sections tend to behave as circular (see how these sections improve the compressive strength up to 46% more than the value which is given by the Eurocode). Contrarily, in case of circular CFT sections, the introduction of these plates implies a decrement of ductility (see Section 6.2) that leads also to a decrement of the confinement effect over the core. This is the reason why the Eurocodes provide an un-conservative design value for circular stiffened sections and it should be revised for these cases.

9. Conclusions

This study aims to describe the influence of stiffening plates in circular and square CFT sections, subjected to large deformation axial loading (up to the collapse of the section). The fact of having these embedded plates have a clear influence not only on the compressive strength, but also on ductility; it is derived from this numerical analysis that the presence of these plates is not always efficient in terms of sectional optimization.

The first conclusion which can be stated from this study is that stiffening plates in circular tubes do not allow a uniform distribution of hoop stress along the tube, so that the confinement effect over the core and the ductility become reduced in all cases. This means that the proposed alternative of introducing embedded plates in circular CFT sections with the aim of saving material is not really efficient, under large monotonic compression. Since the confinement effect depends directly on the shape of the section, the tubular geometry is the most efficient one in order to generate a uniform pressure over the concrete, and to maximize the ductility.

The second conclusion of this research and the most important one is that, contrarily to the case of circular sections, stiffening plates provide a beneficial influence on the compressive response of square-shaped CFT sections in all cases as they avoid the local buckling. The ductility and the strength of all the sections which have been analysed have been enhanced by the presence of one, two or four embedded plates, independently on the outer thickness of the tube. This fact can be explained because these plates provide a high grade of rigidity to the flanges of square-shaped

tubes. The rigidity of the flanges implies a clear growth of the confinement effect over the core that leads directly to an increment of strength.

By comparing circular with square-shaped tubes, it can be also stated that strongly stiffened square-shaped sections (with two or more inner plates) behave in a very similar way to those perfectly circular, in terms of confinement and ductility: even the failure mode follows the typical elephant foot shape as in case of circular CFT sections, as it can be observed in Fig. 25 from Section 6.

Derived from the sections which have been analysed, it can be derived that as thicker is the tube, higher is the influence of stiffeners on confinement and compressive strength (diagram of Fig. 19). Contrarily, as thinner is the outer tube, higher is the influence of these plates on the ductility of the composite section (diagram of Fig. 24). This phenomenon leads to propose this plates for thin-walled square-shaped tubes in all cases, while this solution is only suitable to improve the compressive strength in thick-walled tubes (since it may involve a decrement of ductility in some cases).

Nevertheless, it is important to remember that this investigation is focussed on the efficiency of stiffeners in CFT sections, but always compared with unstiffened ones by assuming an equivalent area of steel and concrete. This fact means that the conclusions stated before refer to equivalent sections in terms of area. Needless to say that the addition of stiffeners in a section without a reduction of the wall-thickness of the outer tube leads always to an improvement of the compressive response of the section. In this case, this is caused by the increment of steel area in the cross-section.

Finally, stiffening plates in CFT sections are interesting for many other reasons. This study is focussed on the influence of these plates on large axial loading response without eccentricity, but stiffeners are beneficial also under other points of view. As the Japanese Zhanfei and Yamao (2011) pointed out for hollow tubes, this solution seems to be especially interesting under cyclic loading also for concrete-filled tubes. The next step in this research is to spread the analyses under different loading cases (combined compression and bending) and also cyclic loading.

References

Brockenbrough, R.L. (1999), Structural Steel Designer's Handbook, (3rd Edition), McGraw Hill, Inc.

Cai, J. and Long, Y.L. (2009), "Local buckling of steel plates in rectangular CFT columns with binding bars", *J. Construct. Steel Res.*, **65**(4), 965-972.

Chacón, R., Mirambell, E. and Real, E. (2012), "Local buckling in concrete-filled circular tubes (CFT)", *Tub. Structures XIV*, pp. 35-42.

Elchalakani, M., Zhao, X.L. and Grzebieta, R.H. (2001), "Concrete-filled circular steel tubes subjected to pure bending", *J. Construct. Steel Res.*, **57**(11), 1141-1168.

Eurocode 4 (2004), EN 1994-1-1:2004, Design of composite steel and concrete structures, Part 1.1: General rules and rules for buildings; European Committee for Standardization, Brussels, Belgium.

Hajjar, J., Schiller, P.H. and Molodan, A. (1998), "A distributed plasticity model for concrete-filled steel tube beam-columns with interlayer slip", *Eng. Struct.*, **20**(8), pp. 663-676

Hu, H., Huang, C., Wu, M. and Wu, Y. (2003), "Nonlinear analysis of axially loaded concrete-filled tube columns with confinement effect", *J. Struct. Eng.*, **129**(10), 1322-1329.

Huang, C.S., Yeh, Y-K., Liu, G-Y., Hu, H., Tsai, K.C., Weng, Y.T., Wang, S.H. and Wu, M.H. (2002), "Axial load behavior of stiffened concrete-filled steel columns", *J. Struct. Eng.*, **128**(9), 1222-1230.

Jankowiak, T. and Lodigowsky, T. (2005), "Identification of parameters of concrete damage plasticity constitutive model", *Found. Civil Environ. Eng.*, Poznan University of Technology.

Liu, G.Y., Yeh, Y.K. and Huang, C.S. (2002), "Tie-bar stiffening scheme for square CFT beam-columns with high tube width-to-thickness ratio", National Science Council Paper; Taipei, Taiwan.
Liu, D., Gho, W. and Yuan, J. (2003), "Ultimate capacity of high-strength rectangular concrete-filled steel hollow section stub columns", *J. Construct. Steel Res.*, **59**(12), 1499-1515.
Lubliner, J. and Oller, S. (1985), "A plastic-damage model for concrete", *Int. J. Solid. Struct.*, **25**(3), 299-326.
Nassem Baig, M., Fan, J. and Nie, J. (2006), "Strength of concrete filled steel tubular columns", *Tsinghua Sci. Technol.*, **11**(6), 657-666.
Ren, Q., Han, L.H., Lam, D. and Hou, C. (2014), "Experiments on special-shaped CFST stub columns under axial compression", *J. Construct. Steel Res.*, **98**, 123-133.
Schneider, S.P. (1998), "Axially loaded concrete-filled steel tubes", *J. Struct. Eng.*, **124**(10), 1125-1138.
Susantha, K.A.S., Ge, H. and Usami, T. (2000), "Uniaxial stress-strain relationship of concrete confined by various shaped steel tubes", *Eng. Struct.*, Nagoya University, **23**(10), 1331-1347.
Tao, Z., Han, L.H. and Wang, Z.B. (2005). "Experimental behaviour of stiffened concrete-filled thin-walled hollow steel structural (HSS) stub columns", *J. Construct. Steel Res.*, **61**(7), 962-983.
Tao, Z., Han, L.H. and Wang, D.Y. (2007). "Experimental behaviour of concrete-filled stiffened thin-walled steel tubular columns", *Thin-Wall. Struct.*, **45**(5), 517-527.
Tao, Z., Han, L H. and Wang, D.Y. (2008). "Strength and ductility of stiffened thin-walled hollow steel structural stub columns filled with concrete", *Thin-Wall. Struct.*, **46**(10), 1113-1128.
Yamao, T., Iwatsubo, K., Yamamuro, T., Ogushi, M. and Matsumura, S. (2002), "Steel bridge piers with inner cruciform plates under cyclic loading", *Thin-Wall. Struct.*, **40**(2), 183-193.
Zhanfei, W. and Yamao, T. (2011), "Ultimate strength and ductility of stiffened steel tubular bridge piers", *Int. J. Steel Struct.*, **11**(1), 81-90.
Zhong, T., Han, L.H. and Wang, Z. (2005), "Experimental behaviour of stiffened concrete-filled thin-walled hollow steel structural (HSS) stub columns", *J. Construct. Steel Res.*, **61**(7), 962-983.
Zhong, T., Han, L.H. and Wang, D. (2007), "Experimental behaviour of concrete-filled stiffened thin-walled steel tubular columns", *Thin-Wall. Struct.*, **45**(5), 517-527.
Zhong, T., Han, L.H. and Wang, D. (2008), "Strength and ductility of stiffened thin-walled hollow steel structural stub columns filled with concrete", *Thin-Wall. Struct.*, **46**(10), 1113-1128.

DL